2019 SECED Conference
Earthquake risk and engineering towards a resilient world
9-10 September 2019, Greenwich, London

SEISMIC PERFORMANCE OF CYLINDRICAL LATTICE SHELLS

Francisco CEDRÓN[1] & Ahmed Y. ELGHAZOULI[2]

Abstract: *Due to their favourable geometric, structural, and aesthetic properties, cylindrical lattice shells are often employed as roofs over large rectangular open spaces like gymnasia or train stations. Whilst their behaviour and design under gravity loads have been widely investigated, their seismic performance has received less attention, particularly in terms of practical design. Currently, European design codes do not include specific provisions for such structural forms. This paper offers insights into the behaviour of cylindrical lattice shells when subjected to seismic loading, with a view towards providing practical seismic design and assessment procedures. Using the finite element program OpenSees, pushover analyses are firstly utilised to examine the nonlinear inelastic static response of shells of various geometrical configurations. Incremental dynamic analyses are then used, considering both material and geometric nonlinearities, to assess the behaviour of shell structures at various performance levels under horizontal and vertical earthquake excitations. Considering a number of key response parameters, it is shown that the behaviour of the shells is greatly dependant on specific geometric parameters which can be used to characterise their seismic performance.*

Introduction

Due to their efficiency in spanning large distances without intermediate columns, and their aesthetic appeal, cylindrical lattice shells are frequently used to cover large rectangular open spaces like sports halls. They are shell structures formed by a triangulated lattice of short steel bars, typically circular hollow sections, which are held together by fixed nodes that provide bending resistance against buckling.

Cylindrical lattice shells are commonly designed mainly against gravity loads, as their geometry is suited to resist these forces. However, the actions produced by seismic events can have a significant impact on their performance and member sizes, and must be accounted for. Their design against gravity loads and buckling has been covered extensively in previous studies (Makowski, 1985; Gioncu, 1995; Dulácksa and Kollár, 2000; Bulenda and Knippers, 2001; Yamada, 2012). Their dynamic properties have been studied parametrically previously (Shen et al., 2003; Chen et al., 2005). These studies also suggest seismic force coefficients derived by dividing the forces experienced from seismic actions compared to those from gravity loads, and obtaining amplification ratios. However, recent reviews of the state of the art on the seismic design of lattice shells (Nakazawa et al., 2012) do not show a consensus on an accepted way for designing these structures against earthquake actions. Furthermore, European codes of practice (Eurocode 8, 2004) currently lack specific provisions for the seismic design of lattice shells. The lack of guidance in design codes leads designers to perform complex analyses to design them, or just design them to remain elastic.

This paper delves into the seismic performance of single layer cylindrical lattice shells, with the aim of shedding light on their post-elastic behaviour, and outlining the main geometric properties that influence their response under earthquake excitations.

Structural configuration

Geometry

The structures examined in this paper are single layer cylindrical lattice shells. The key parameters that define their geometry are the span, B, the rise, H, and the length, L. The rise and the span of the shell define three points that form a circular arc. The nodes of the edge arches are then located on this arc, at equal distances, with the number of divisions labelled

[1] PhD Candidate, Imperial College London, London, UK, pancho.cedron12@imperial.ac.uk
[2] Professor, Imperial College London, London, UK

n_{div}. These nodes are then joined by straight members. The arc is then extruded along the length L, and is divided longitudinally into n_{long} divisions, forming a triangulated grid.

The angle formed by the longitudinal members and the diagonal members is denoted α. Two important ratios are derived from the basic key geometric parameters. These are the rise to span ratio, labelled H/B, and the length to span ratio, L/B. The X-direction corresponds to the transversal direction, parallel to the edge arches, the Y-direction is the longitudinal, and the Z-direction is the vertical. The geometry of the shell and the parameters that define it are depicted in Figure 1.

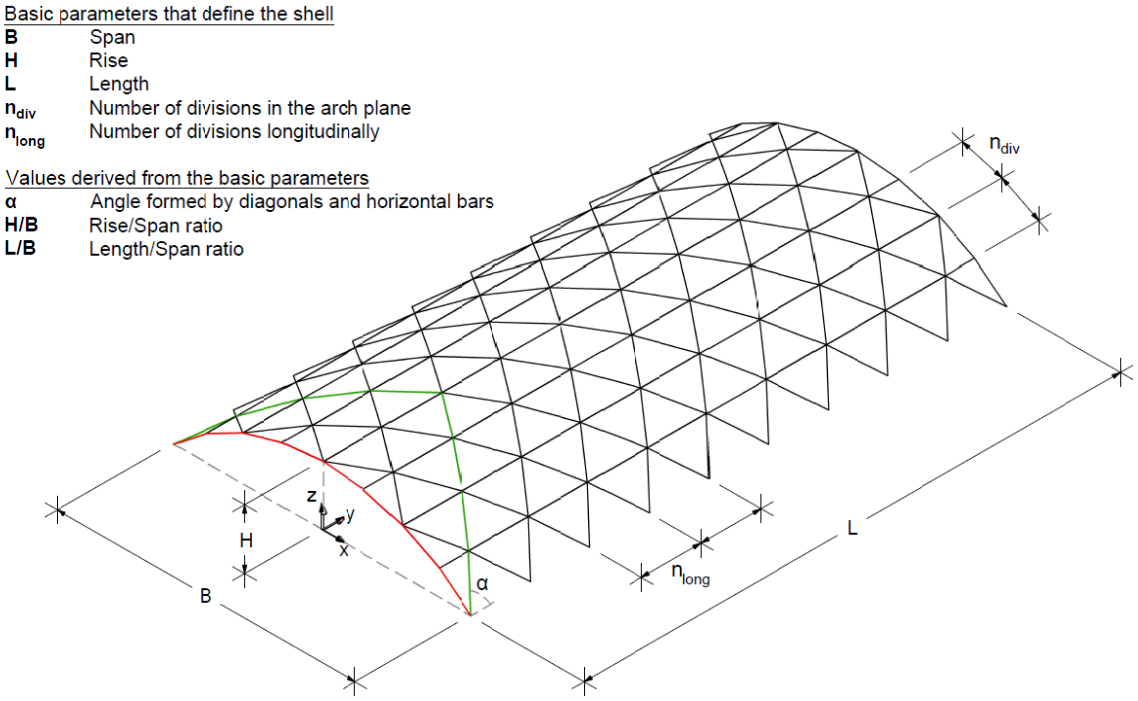

Figure 1. Key parameters that define the geometry of the study shells

Boundary conditions and loading

The boundary conditions considered in this paper have been chosen to reflect practical ranges. The longitudinal edges of the shells are pinned along their length, restraining movements in all three directions, but allowing rotations in any direction. The edge arches are unrestrained, free to move and rotate, as would be the case were there an opening in that plane, or a non-structural glass façade.

Gravity loading is considered by applying a vertical surface load, *q*, given in kN/m², to take into account superimposed dead loads, live loads, or snow loads. This surface load is then multiplied by the tributary area of each node, and applied on each node as a vertical point load. These loads add to the mass of the structure, and are computed as such for the dynamic analyses, where the masses are modelled as lumped at the nodes.

Model definition

The open source earthquake engineering software *OpenSees* (McKenna, 2006) was used for modelling the shells and their analysis. The members are modelled using force-based beam column elements. These include geometric nonlinearities by using the *Co-rotational* geometric transformation, and they incorporate material nonlinearities by modelling the circular hollow sections using fibre sections, with the uniaxial material *Steel02* (Filippou, 2012), a Young's Modulus of E = 210,000 N/mm², a yield strength of f_y = 275 N/mm², and a strain hardening ratio of 0.5%. Rayleigh damping was used for the dynamic analysis, with a damping ratio of ζ = 0.02.

Linear elastic response

Shell design

Five shells of H/B from 0.1 to 0.5 were selected and designed following conventional shell buckling design recommendations (Kollár and Dulácksa, 1984; Kato, 2014). Their span, B, is 15 m, and their length, L, is 27 m. The shells were initially designed for self-weight, a superimposed dead load of 1.0 kN/m², and a live load of 1.0 kN/m². Using SAP2000 (CSI, 2018), and following Eurocode provisions (Eurocode 3, 2005), a load combination of 1.35 Dead Load + 1.50 Live Load was considered, as well as a load combination of 1.0 Dead Load + 0.30 Live Load + 1.0 Earthquake Load, obtained from an equivalent horizontal force procedure using Eurocode 8 parameters of a_g = 0.25 g, Spectrum Type 1, and ground type C. Only two member sizes were used: a circular hollow section for longitudinal members, and another for the diagonals. The resulting member sizes and shell characteristics are given in Table 1.

Rise/Span Ratio (H/B)	0.1	0.2	0.3	0.4	0.5
Longitudinal members	60×4	60×4	60×4	60×4	60×4
Diagonal members	165×4	141×4	140×4	151×4	174×4
1st mode period, T_1 (s)	0.558	0.877	1.212	1.547	1.512
1st mode mass participation, UX	0.122	0.389	0.640	0.809	0.901

Table 1. Member sizes and shell characteristics

Record selection

A suite of seven unaltered earthquake records has been selected from the PEER NGA West database (Ancheta et al., 2014) to represent a medium seismic hazard for Europe. The records selected have a magnitude M between 5.0 and 6.5, distance from the fault ranging from 10 km to 100 km, and a shear wave velocity V_s from 180 m/s to 800 m/s. A matching procedure minimized the root mean square difference from the target Eurocode 8 Type 1 Spectrum with Soil Type C, over the period range of 0.2 s to 2.0 s. The seven records selected and their seismological characteristics are shown in Table 2 below.

Record No.	Earthquake Name	M	Distance (km)	V_{S30} (m/s)	PGA (g)	Scale Factor	D_{RMS}
00564L	Kalamata, Greece	6.2	11.2	339	0.26	1.23	0.188
00127T	Friuli, Italy	5.5	15.1	339	0.05	7.55	0.197
00299L	Irpinia, Italy	6.2	41.7	500	0.04	9.83	0.226
00302T	Irpinia, Italy	6.2	22.7	530	0.11	3.49	0.230
01137T	Dinar, Turkey	6.4	35.6	339	0.04	7.16	0.245
00130L	Friuli, Italy	5.9	14.3	339	0.11	3.03	0.246
00481L	Lazio-Abruzzo, Italy	5.8	45.5	339	0.04	9.25	0.254

Table 2. Records selected for the analyses

Shell response to earthquake loading

The horizontal and vertical components of the seven selected records were applied, with the horizontal components scaled to match the spectrum using the scale factors in Table 2, and the vertical components scaled so that the vertical acceleration a_{vg}/a_g = 0.90, as per Eurocode 8 provisions. The average of the maximum axial forces and bending moments experienced in each the seven records was taken. The values of axial forces along the diagonals shown in green in Figure 1 are compared, as these are the members where the highest axial forces are found for every load case. The values of bending moments compared are from the edge arches, shown in red in Figure 1, as these experience the highest bending moments.

Figure 2 shows the plots of axial force utilisation, defined as the axial force, N, divided by the axial capacity of the member, $N_{pl} = A \cdot f_y$, for the gravity load case, the horizontal and vertical components independently, or both components acting simultaneously, for three representative shells. The axial forces produced by the ultimate load in the gravity load case are higher than those from the earthquake cases. The reduction in applied gravity load considered in the seismic cases reduces the axial demands significantly, and the ground accelerations at this level of seismic hazard still do not produce axial forces of greater magnitude than those produced by the gravity load case. Comparing the two directional components, for all cases, the vertical excitation produces higher axial forces than the horizontal component, particularly so in

shells of low H/B. The magnitude of the axial forces is greatest for these shallow shells, ranging between 0.15 and 0.30 of section axial utilisation, compared to values of 0.03-0.13 for the shell of H/B = 0.5.

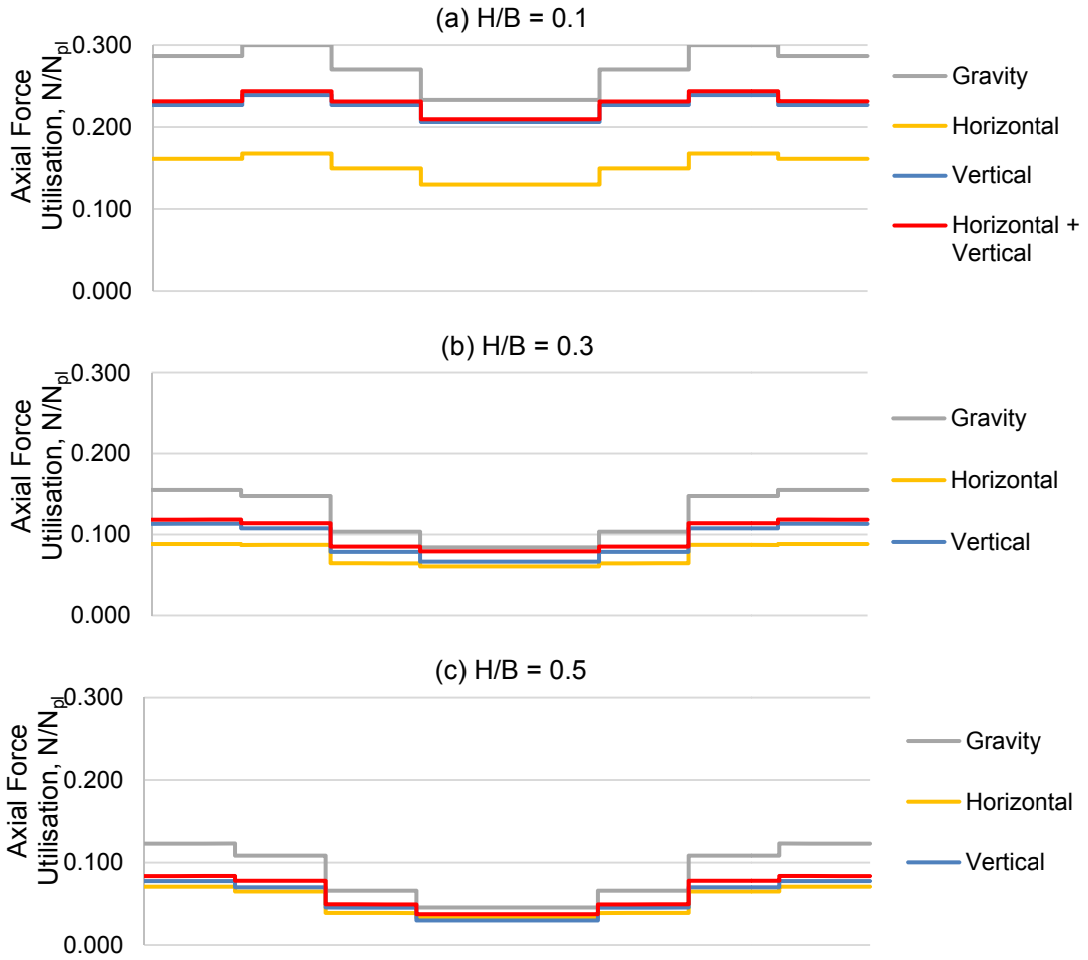

Figure 2. Axial Force Utilisation for shells of (a) H/B = 0.1, (b) H/B = 0.3, and (c) H/B = 0.5

Figure 3 shows the plots of bending moment utilisation, defined as the bending moment, M, divided by the plastic moment capacity of the section, $M_{pl} = W_{pl} \cdot f_y$. Contrary to the axial forces, for the bending moments, the horizontal excitations produce higher bending moments than the gravity or vertical excitation cases. The vertical earthquake produces higher bending moments than the gravity load case for the shell of H/B = 0.1, indicating that shells of lower H/B are more vulnerable to vertical effects as expected. Nevertheless, the bending moments found in shells of H/B ratio are smaller, reaching up to only 0.30 of M_{pl}, compared to those in shells of high H/B, reaching up to 0.90 M_{pl}. The initial design of the shallower shells was largely governed by global buckling under gravity loads, and hence they show a larger overstrength in the seismic cases.

The way the bending moments are distributed also differs between the horizontal and vertical earthquake cases. Both excitations produce a peak in the joint between the second and third members of the edge arch. However, for the horizontal earthquake case, the entire member and the next joint experience bending moments that are similar in magnitude, and then decrease towards the centre. These correspond to the members with the largest displacement in the first mode shape. On the other hand, the vertical excitations produce a second, more concentrated peak of bending moments in the centre of the shell.

The internal forces produced by the simultaneous action of the horizontal and vertical components are not very different to those produced by the vertical component alone for the axial forces, or to those produced by the horizontal component for the bending moments. This indicates that the horizontal and vertical excitations are producing largely uncoupled responses, as the frequencies they are influencing are different.

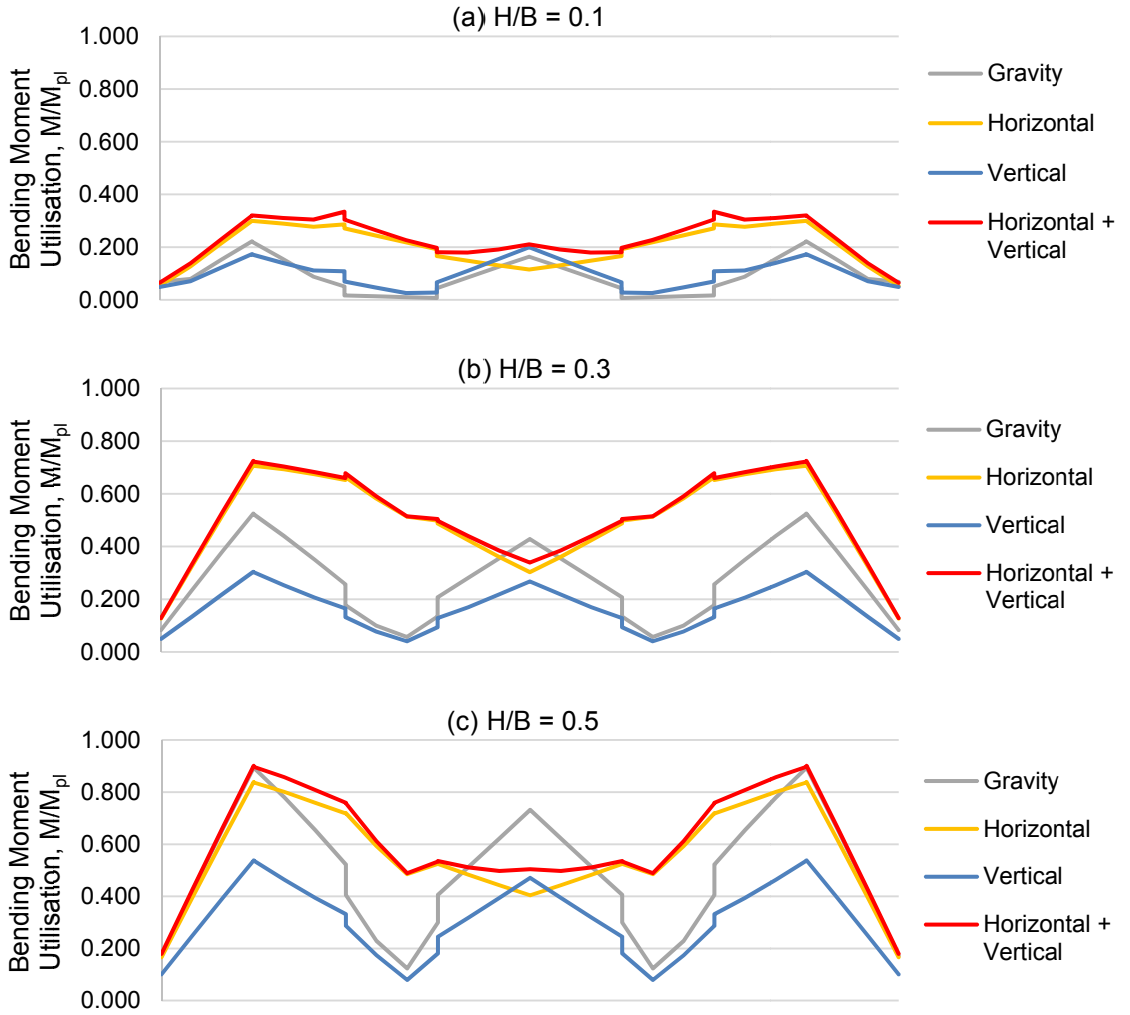

Figure 3. Bending Moment Utilisation for shells of (a) H/B = 0.1, (b) H/B = 0.3, and (c) H/B = 0.5

Nonlinear Static Analysis

In order to gain insight into the nonlinear behaviour of the shells, a series of nonlinear static, or pushover, analyses have been carried out using OpenSees. In an initial step, the loads due to gravity are applied, with the load case of 1.0·Dead Load + 0.30·Live Load. Then, the lateral loads are applied, using forces proportional to the first mode shape. The structures are pushed, and the horizontal X displacement of the top node of the edge arch is monitored, until failure of the shell is reached, or the analysis fails to converge. The horizontal drift is defined as the horizontal displacement of the top node of the edge arch divided by the rise of the shell.

Figure 4 shows the pushover curves for the five shells studied. In order to determine where significant changes in behaviour occur, to establish key limit points, several points are marked on the curves. The first point, shown in green, marks the point at which any one member in the edge arch reaches its elastic moment capacity, M_{el}. The second point takes into account the interaction of forces through the following equation:

$$\frac{M_y}{M_{y,pl,d}} + \frac{M_z}{M_{z,pl,d}} + \left(\frac{N}{N_{pl,d}}\right)^2 \leq 1 \qquad (1)$$

This point, shown in cyan, marks the moment at which a member of the edge arch exceeds this check. The third point, shown in red, indicates when the full plastic moment capacity, M_{pl}, has been reached in a member of the edge arch. Finally, the point marked in dark blue signals the point at which the critical strain, ε_{cr}, is first reached in a member. This would represent when the cross section is predicted to undergo local buckling, a phenomenon dependent on the diameter,

D, and thickness, t, of the section. This critical strain is determined from the elastic critical buckling stress of a circular hollow section, from the following equation (Buchanan et al., 2016):

$$\varepsilon_{cr} = \frac{\varepsilon_y}{f_y} \cdot \frac{E}{\sqrt{3 \cdot (1 - \nu^2)}} \cdot \frac{2t}{D} \tag{2}$$

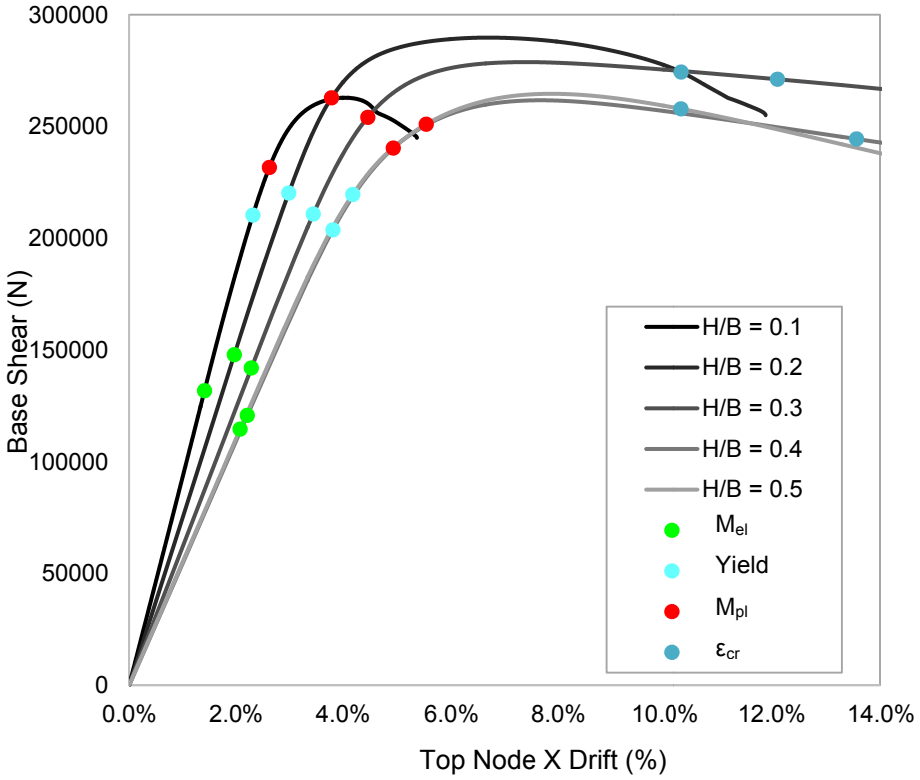

Figure 4. Pushover curves for five shells studied, showing key points.

From Figure 4, it is clear that the shells continue to act in a linear fashion when the elastic moment is reached in one of the edge arch members. The first significant deviation from linearity comes at the cyan point, when one of the members reaches the yield criterion from Equation 1. In the shell of H/B = 0.1, this point is close to the point marked in red, where the plastic moment capacity is reached, indicating that the main axis bending moment is contributing the most to the yielding. In deeper shells, these points are further apart, implying that the minor axis bending effects are more significant.

The nonlinear behaviour of the shells is highly dependent on H/B. The shallower shells experience a relatively rapid collapse, and show less ductility than the shells with higher H/B. Due to their geometry, shallow shells are more prone to buckle and snap through once yielding is initiated, whereas deeper shells behave more like a framed structure, and thus exhibit a more ductile behaviour. In addition, the vertical components of the forces being applied on the shallow shells are larger than the ones on the deeper shells, due to the first mode shape of each structure. These downward forces have a very detrimental effect on the shells of low rise to span ratio, and cause the structure to quickly collapse once the geometry has deformed enough for the structure not to be able to resist the loads working as a shell.

Figure 5 shows the interaction of forces in the edge arches of the five shells at the point of first yield. The first plastic hinge forms in the same place for all of the shells, at the quarter point of the shell, corresponding to the location of highest displacement in the first mode shape. Figure 6 shows the curvature in the edge arches of the shells at the point where the critical strain, ε_{cr}, is reached in one of the members, which could be considered the point of failure of the shells. As the shells go into the nonlinear range, their behaviour is defined more by their rise to span ratio. The shell of H/B = 0.1 concentrates its plasticity in the four plastic hinges formed around its quarter points. In the shells of higher rise to span ratio, plasticity spreads more throughout the shells, forming more plastic hinges in other members, and hence prolonging their ductility.

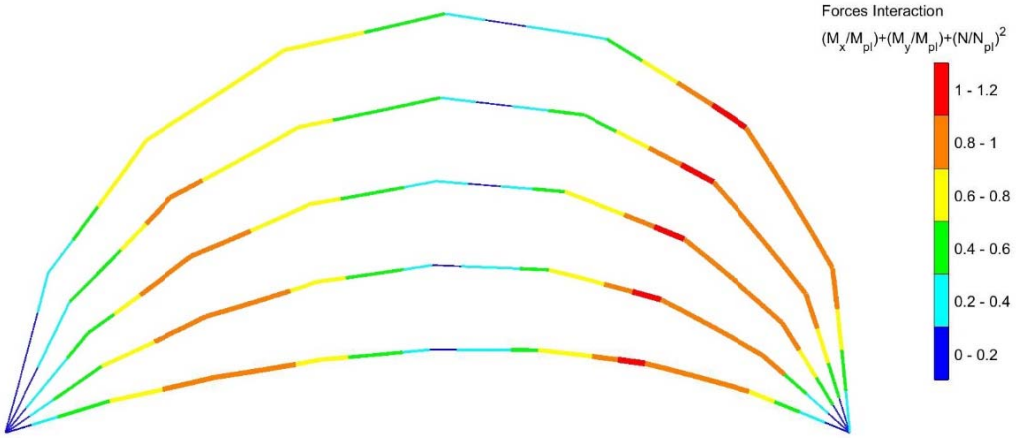

Figure 5. Interaction of forces in the edge arch for the five shells at the point of first yield

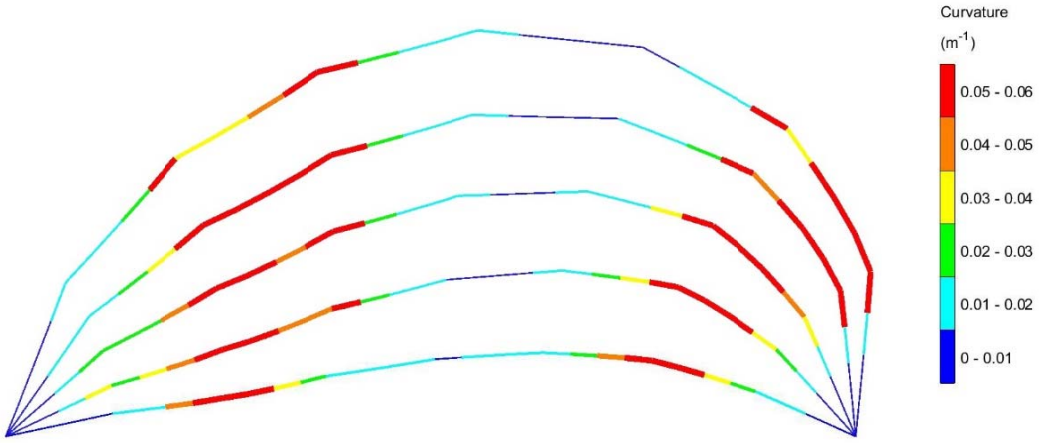

Figure 6. Curvature in the edge arch at point of failure

Table 3 shows the numerical results of the nonlinear static analysis of the five shells studied. The maximum horizontal base shears reached by all the shells range between about 262 kN for the shell of H/B = 0.4 and about 290 kN N for the shell of H/B = 0.2. The overstrength exhibited by the shells, expressed as V_{max}/V_1, is between 1.20 and 1.32. Shells of higher rise to span ratio have less reserve capacity in terms of reaching increased base shear after first yield; however, they are able to maintain the level of base shear reached for larger levels of deformation than shells of lower rise to span ratio, showing better ductility.

Rise to Span ratio, H/B		**0.1**	**0.2**	**0.3**	**0.4**	**0.5**
Height, h (m)		1.50	3.00	4.50	6.00	7.50
Base Z Reaction, P_{tot} (N)		54230	570931	629524	711461	814819
Maximum Base Shear, V_{max} (N)		262860	289763	278815	261732	264626
At 1st Yield	Base Shear, V_1 (N)	210369	220200	210842	203788	219614
	Top Node X Displacement, d_r (m)	0.035	0.089	0.155	0.228	0.313
	Top Node X Drift (%)	2.31%	2.98%	3.44%	3.80%	4.17%
	V_{max}/V_1	1.25	1.32	1.32	1.28	1.20
	Drift sensitivity coefficient, θ	0.06	0.08	0.10	0.13	0.15

Table 3. Nonlinear static analysis results

The drift sensitivity coefficient, θ, which Eurocode 8 uses to determine the influence of second-order effects was calculated at the point of first yield. This was done taking the displacement of the top node of the edge arch d_r, the total weight of the structure, P_{tot}, the rise of the structure, h, and the base shear at the point of first yield, V_1, using the following equation:

$$\theta = \frac{P_{tot} \cdot d_r}{V_{tot} \cdot h} \tag{3}$$

Eurocode 8 stipulates that second-order effects need not be taken into account if this value is not greater than 0.10. This is the case for the shells of low rise to span ratio. Shells with H/B of 0.4 and above will be vulnerable to second-order effects according to this measure.

Incremental Dynamic Analysis

To get a detailed picture of the nonlinear behaviour of single layer cylindrical lattice shells, the same five shells were studied through numerous nonlinear time history analyses using the incremental dynamic analysis (IDA) methodology (Vamvatsikos, 2002). In order to assess the influence of the vertical component of the earthquakes on the results, two sets of analyses were carried out. In the first one, only the horizontal component of the earthquake was applied. In the second one, both the horizontal and the vertical component of the earthquake were used. The actual vertical components from each respective earthquake were used, and these were scaled by the same scaling factor as the horizontal component, in an attempt to keep the loading associated with real events.

The IDA curves showing the progression of drift as the records are scaled up are presented in Figure 7 for the five shells of varying H/B. The peak ground acceleration was chosen as the intensity measure, as it presented less dispersion between the runs from the different records when compared to the first mode spectral acceleration, especially for the shallower shells. The thin lines represent the seven individual runs for each earthquake record, where the grey curves are the IDAs using just horizontal excitations, and the red curves include both the horizontal and vertical component of the earthquakes. To summarise the results, the median curves, as well as the 16% and 84% fractile curves are also included.

The values of drift reached by the shells are a function of H/B. Higher values are reached by the deeper shells, as was seen in the nonlinear static analyses. In numerous records, and this is captured by some of the medians, a hardening is observed, in that, having reached a certain level of drift at a given PGA, counter-intuitively, some shells then exhibit a lower value of drift at a higher PGA. This is due to the nature of the IDA, where, as the records are scaled upwards, an early cycle from a record that initially did not cause yielding, triggers inelasticity earlier on, changing the properties of the shell for the subsequent cycles of that same record, and thus eliciting a different response. In some cases, this response results in a smaller damage measure, as the structure is somewhat protected from the later cycles of higher amplitude by the early yielding. With an increased number of records, a smoother median curve would predictably be obtained. Conversely, much higher values of PGA are reached in the shallow shells, exhibiting a much stiffer response than those of high H/B.

When comparing the response of shells subjected to horizontal excitations only against those subjected to horizontal and vertical excitations simultaneously, the geometry of the shells once again plays an important role. The shells of low rise to span ratio present the highest difference between their two responses. The vertical component of the earthquake affects these structures greatly, leading to a full collapse of the structure at a much lower value of peak ground acceleration when including the vertical accelerations in the shell of H/B = 0.1. This difference exists in the rest of the shells, but it is not as pronounced. Shells of higher rise to span ratios tend to be less affected by the vertical component. However, their collapse is brought about at a much lower peak ground acceleration. This is due to the overstrength in the shallow shells, where buckling was a more decisive factor when sizing their members during their design.

Concluding Remarks

This paper examined the seismic performance of single layer cylindrical lattice shells. Their response in the linear elastic range was first examined. The highest concentration of internal forces occurred in the edge arches. On the other hand, the bending moments as a whole were found to be more significant than the axial forces, and highest at the quarter points of the shells.

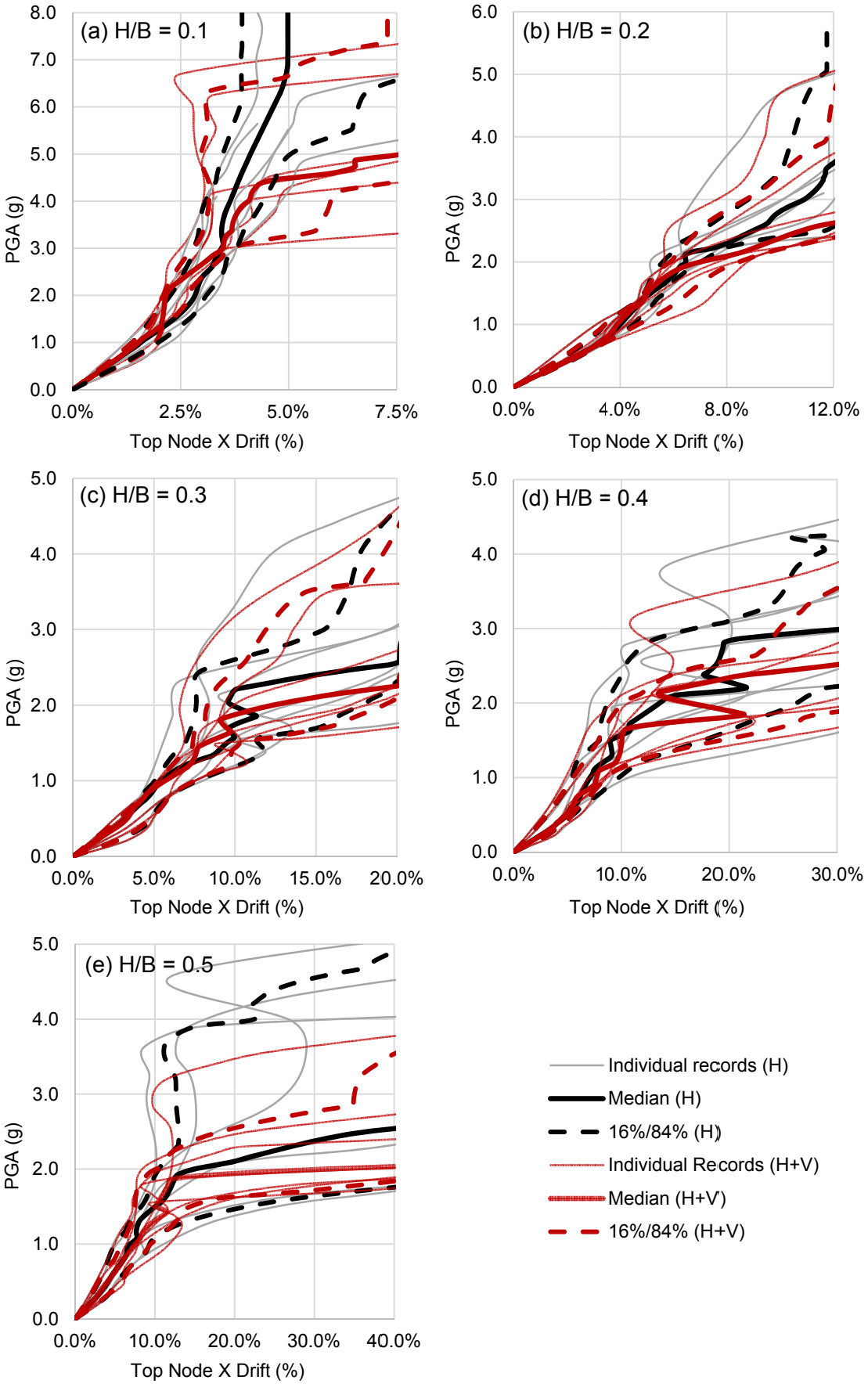

Figure 7. Results for the Incremental Dynamic Analysis performed on the five shells

The rise to span ratio had a significant influence on the response of the shells. Shallower shells exhibited a stiffer response, with higher axial forces, and the possibility of snap-through behaviour as displacements increased past the linear range. Deeper shells showed more ductility, with higher bending moments and much larger levels of drift. Importantly, the influence of the vertical earthquake component was shown to be particularly significant in shells of low rise to span ratios. Accordingly, multi-directional seismic excitation effects should be accounted for within assessment and design procedures. Further detailed investigations are currently underway with a view to providing guidance on detailed seismic analysis procedures as well as simplified design approaches which are suitable for implementation in codes of practice.

References

ANCHETA, T. D., DARRAGH, R. B., STEWART, J. P., SEYHAN, E., SILVA, W. J., CHIOU, B. S.-J., WOODDELL, K. E., GRAVES, R. W., KOTTKE, A. R., BOORE, D. M., KISHIDA, T. & DONAHUE, J. L. 2014. NGA-West2 Database. *Earthquake Spectra,* 30**,** 989-1005.

EUROCODE 8. 2004. BS EN 1998-1. Design of structures for earthquake resistance. *Part 1: General rules, seismic actions and rules for buildings.* British Standards Institution.

EUROCODE3. 2005. BS EN1993-1. Design of steel structures. *Part 1.1: General rules and rules for buildings.* British Standards Institution.

BUCHANAN, C., GARDNER, L. & LIEW, A. 2016. The continuous strength method for the design of circular hollow sections. *Journal of Constructional Steel Research,* 118**,** 207-216.

BULENDA, T. & KNIPPERS, J. 2001. Stability of grid shells. *Computers and Structures,* 79**,** 1161-1174.

CHEN, Y. B., LI, Q. S. & CHEN, J. M. 2005. Dynamic characteristics of single-layer cylindrical lattice shells. *Proceedings of the ICE - Structures and Buildings,* 158**,** 41-51.

CSI 2018. SAP2000 Integrated Software for Structural Analysis and Design. Berkeley, California: Computers and Structures Inc.

DULÁCKSA, E. & KOLLÁR, L. 2000. Buckling analysis of reticulated shells. *International Journal of Space Structures,* 15**,** 195-203.

FILIPPOU, F. 2012. *Steel02 Material -- Giuffré-Menegotto-Pinto Model with Isotropic Strain Hardening* [Online]. OpenSees. Available: http://opensees.berkeley.edu/wiki/index.php/Steel02_Material_--_Giuffr%C3%A9-Menegotto-Pinto_Model_with_Isotropic_Strain_Hardening [Accessed 2018].

GIONCU, V. 1995. Buckling of reticulated shells, state of the art. *International Journal of Space Structures,* 10**,** 1-46.

KATO, S. 2014. *Guide to Buckling Load Evaluation of Metal Reticulated Roof Structures*, IASS Working Group 8.

KOLLÁR, L. & DULÁCKSA, E. 1984. *Buckling of Shells for Engineers,* New York, John Wiley & Sons.

MAKOWSKI, Z. S. (ed.) 1985. *Analysis, design and construction of braced barrel vaults,* London: Elsevier Applied Science Publishers.

MCKENNA, F. 2006. *Open System for Earthquake Engineering Simulation* [Online]. Available: http://opensees.berkeley.edu/ [Accessed 2016].

NAKAZAWA, S., KATO, S., TAKEUCHI, T., XUE, S.-D. & LAZARO, C. 2012. State-of-the-art of seismic response evaluation methods for metal roof spatial structures. *Journal-International Association for Shell and Spatial Structures,* 53**,** 117-130.

SHEN, S., XING, J. & FAN, F. 2003. Dynamic behavior of single-layer latticed cylindrical shells subjected to seismic loading. *Earthquake Engineering and Engineering Vibration,* 2**,** 269-279.

VAMVATSIKOS, D. C., C. ALLIN 2002. Incremental dynamic analysis. *Earthquake Engineering and Structural Dynamics*, 491-514.

YAMADA, S. 2012. Buckling load evaluation method for single layer cylindrical lattice shells. *Journal of Civil Engineering and Architecture,* 6**,** 268.